

First Muon-Neutrino Disappearance Study with an Off-Axis Beam

K. Abe,^{49,*} N. Abgrall,¹⁶ Y. Ajima,^{18,†} H. Aihara,^{48,*} J.B. Albert,¹³ C. Andreopoulos,⁴⁷ B. Andrieu,³⁷
M.D. Anerella,⁶ S. Aoki,²⁷ O. Araoka,^{18,†} J. Argyriades,¹⁶ A. Ariga,³ T. Ariga,³ S. Assylbekov,¹¹ D. Autiero,³²
A. Badertscher,¹⁵ M. Barbi,⁴⁰ G.J. Barker,⁵⁶ G. Barr,³⁶ M. Bass,¹¹ M. Batkiewicz,¹⁷ F. Bay,³ S. Bentham,²⁹
V. Berardi,²² B.E. Berger,¹¹ I. Bertram,²⁹ M. Besnier,¹⁴ J. Beucher,⁸ D. Beznosko,³⁴ S. Bhadra,⁶⁰ F.d.M. Blaszczyk,⁸
A. Blondel,¹⁶ C. Bojecho,⁵³ J. Bouchez,^{8,‡} S.B. Boyd,⁵⁶ A. Bravar,¹⁶ C. Bronner,^{14,28} D.G. Brook-Roberge,⁵
N. Buchanan,¹¹ H. Budd,⁴¹ R. Calland,³⁰ D. Calvet,⁸ J. Caravaca Rodríguez,¹⁹ S.L. Cartwright,⁴⁴ A. Carver,⁵⁶
R. Castillo,¹⁹ M.G. Catanesi,²² A. Cazes,³² A. Cervera,²⁰ C. Chavez,³⁰ S. Choi,⁴³ G. Christodoulou,³⁰ J. Coleman,³⁰
G. Collazuol,²⁴ W. Coleman,³¹ K. Connolly,⁵⁷ A. Curioni,¹⁵ A. Dabrowska,¹⁷ I. Danko,³⁸ R. Das,¹¹ G.S. Davies,²⁹
S. Davis,⁵⁷ M. Day,⁴¹ G. De Rosa,²³ J.P.A.M. de André,¹⁴ P. de Perio,⁵¹ T. Dealtry,^{36,47} A. Delbart,⁸ C. Densham,⁴⁷
F. Di Lodovico,³⁹ S. Di Luise,¹⁵ P. Dinh Tran,¹⁴ J. Dobson,²¹ U. Dore,²⁵ O. Drapier,¹⁴ T. Duboyski,³⁹
F. Dufour,¹⁶ J. Dumarchez,³⁷ S. Dytman,³⁸ M. Dziewiecki,⁵⁵ M. Dziomba,⁵⁷ S. Emery,⁸ A. Ereditato,³
J.E. Escallier,⁶ L. Escudero,²⁰ L.S. Esposito,¹⁵ M. Fechner,^{13,8} A. Ferrero,¹⁶ A.J. Finch,²⁹ E. Frank,³ Y. Fujii,^{18,†}
Y. Fukuda,³³ V. Galymov,⁶⁰ G.L. Ganetis,⁶ F. C. Gannaway,³⁹ A. Gaudin,⁵³ A. Gendotti,¹⁵ M.A. George,³⁹
S. Giffin,⁴⁰ C. Giganti,¹⁹ K. Gilje,³⁴ A.K. Ghosh,⁶ T. Golan,⁵⁹ M. Goldhaber,^{6,‡} J.J. Gomez-Cadenas,²⁰ S. Gomi,²⁸
M. Gonin,¹⁴ N. Grant,²⁹ A. Grant,⁴⁶ P. Gumplinger,⁵² P. Guzowski,²¹ D.R. Hadley,⁵⁶ A. Haesler,¹⁶ M.D. Haigh,³⁶
K. Hamano,⁵² C. Hansen,^{20,§} D. Hansen,³⁸ T. Hara,²⁷ P.F. Harrison,⁵⁶ B. Hartfel,³¹ M. Hartz,^{60,51} T. Haruyama,^{18,†}
T. Hasegawa,^{18,†} N.C. Hastings,⁴⁰ A. Hatzikoutelis,²⁹ K. Hayashi,^{18,†} Y. Hayato,^{49,*} C. Hearty,^{5,¶} R.L. Helmer,⁵²
R. Henderson,⁵² N. Higashi,^{18,†} J. Hignight,³⁴ A. Hillairet,⁵³ T. Hiraki,²⁸ E. Hirose,^{18,†} J. Holeczek,⁴⁵ S. Horikawa,¹⁵
K. Huang,²⁸ A. Hyndman,³⁹ A.K. Ichikawa,²⁸ K. Ieki,²⁸ M. Ieva,¹⁹ M. Iida,^{18,†} M. Ikeda,²⁸ J. Ilic,⁴⁷ J. Imber,³⁴
T. Ishida,^{18,†} C. Ishihara,⁵⁰ T. Ishii,^{18,†} S.J. Ives,²¹ M. Iwasaki,⁴⁸ K. Iyogi,⁴⁹ A. Izmaylov,²⁶ B. Jamieson,⁵⁸
R.A. Johnson,¹⁰ K.K. Joo,⁹ G.V. Jover-Manas,¹⁹ C.K. Jung,³⁴ H. Kaji,^{50,*} T. Kajita,^{50,*} H. Kakuno,⁴⁸
J. Kameda,^{49,*} K. Kaneyuki,^{50,‡} D. Karlen,^{53,52} K. Kasami,^{18,†} I. Kato,⁵² H. Kawamuko,²⁸ E. Kearns,^{4,*}
M. Khabibullin,²⁶ F. Khanam,¹¹ A. Khotjantsev,²⁶ D. Kielczewska,⁵⁴ T. Kikawa,²⁸ J. Kim,⁵ J.Y. Kim,⁹ S.B. Kim,⁴³
N. Kimura,^{18,†} B. Kirby,⁵ J. Kisiel,⁴⁵ P. Kitching,¹ T. Kobayashi,^{18,†} G. Kogan,²¹ S. Koike,^{18,†} A. Konaka,⁵²
L.L. Kormos,²⁹ A. Korzenev,¹⁶ K. Koseki,^{18,†} Y. Koshio,^{49,*} Y. Kouzuma,⁴⁹ K. Kowalik,² V. Kravtsov,¹¹ I. Kreslo,³
W. Kropp,⁷ H. Kubo,²⁸ J. Kubota,²⁸ Y. Kudenko,²⁶ N. Kulkarni,³¹ Y. Kurimoto,²⁸ R. Kurjata,⁵⁵ T. Kutter,³¹
J. Lagoda,² K. Laihem,⁴² M. Laveder,²⁴ M. Lawe,⁴⁴ K.P. Lee,⁵⁰ P.T. Le,³⁴ J.M. Levy,³⁷ C. Licciardi,⁴⁰ I.T. Lim,⁹
T. Lindner,⁵ C. Lister,⁵⁶ R.P. Litchfield,^{56,28} M. Litos,⁴ A. Longhin,⁸ G.D. Lopez,³⁴ P.F. Loverre,²⁵ L. Ludovici,²⁵
T. Lux,¹⁹ M. Macaire,⁸ L. Magaletti,²² K. Mahn,⁵² Y. Makida,^{18,†} M. Malek,²¹ S. Manly,⁴¹ A. Marchionni,¹⁵
A.D. Marino,¹⁰ A.J. Marone,⁶ J. Marteau,³² J.F. Martin,^{51,¶} T. Maruyama,^{18,†} T. Maryon,²⁹ J. Marzec,⁵⁵
P. Masliah,²¹ E.L. Mathie,⁴⁰ C. Matsumura,³⁵ K. Matsuoka,²⁸ V. Matveev,²⁶ K. Mavrokoridis,³⁰ E. Mazzucato,⁸
N. McCauley,³⁰ K.S. McFarland,⁴¹ C. McGrew,³⁴ T. McLachlan,⁵⁰ M. Messina,³ W. Metcalf,³¹ C. Metelko,⁴⁷
M. Mezzetto,²⁴ P. Mijakowski,² C.A. Miller,⁵² A. Minamino,²⁸ O. Mineev,²⁶ S. Mine,⁷ A.D. Missert,¹⁰ G. Mituka,⁵⁰
M. Miura,^{49,*} K. Mizouchi,⁵² L. Monfregola,²⁰ F. Moreau,¹⁴ B. Morgan,⁵⁶ S. Moriyama,^{49,*} A. Muir,⁴⁶
A. Murakami,²⁸ J.F. Muratore,⁶ M. Murdoch,³⁰ S. Murphy,¹⁶ J. Myslik,⁵³ N. Nagai,²⁸ T. Nakadaira,^{18,†}
M. Nakahata,^{49,*} T. Nakai,³⁵ K. Nakajima,³⁵ T. Nakamoto,^{18,†} K. Nakamura,^{18,**} S. Nakayama,^{49,*} T. Nakaya,^{28,*}
D. Naples,³⁸ M.L. Navin,⁴⁴ T.C. Nicholls,⁴⁷ B. Nielsen,³⁴ C. Nielsen,⁵ K. Nishikawa,^{18,†} H. Nishino,⁵⁰
K. Nitta,²⁸ T. Nobuhara,²⁸ J.A. Nowak,³¹ Y. Obayashi,^{49,*} T. Ogitsu,^{18,†} H. Ohhata,^{18,†} T. Okamura,^{18,†}
K. Okumura,^{50,*} T. Okusawa,³⁵ S.M. Oser,⁵ M. Otani,²⁸ R. A. Owen,³⁹ Y. Oyama,^{18,†} T. Ozaki,³⁵ M.Y. Pac,¹²
V. Palladino,²³ V. Paolone,³⁸ P. Paul,³⁴ D. Payne,³⁰ G.F. Pearce,⁴⁷ J.D. Perkin,⁴⁴ V. Pettinacci,¹⁵ F. Pierre,^{8,‡}
E. Poplawska,³⁹ B. Popov,^{37,††} M. Posiadala,⁵⁴ J.-M. Poutissou,⁵² R. Poutissou,⁵² P. Przewlocki,² W. Qian,⁴⁷
J.L. Raaf,⁴ E. Radicioni,²² P.N. Ratoff,²⁹ T.M. Rauffer,⁴⁷ M. Ravonel,¹⁶ M. Raymond,²¹ F. Retiere,⁵² A. Robert,³⁷
P.A. Rodrigues,⁴¹ E. Rondio,² J.M. Roney,⁵³ B. Rossi,³ S. Roth,⁴² A. Rubbia,¹⁵ D. Ruterbories,¹¹ S. Sabouri,⁵
R. Sacco,³⁹ K. Sakashita,^{18,†} F. Sánchez,¹⁹ A. Sarrat,⁸ K. Sasaki,^{18,†} K. Scholberg,^{13,*} J. Schwehr,¹¹ M. Scott,²¹
D.I. Scully,⁵⁶ Y. Seiya,³⁵ T. Sekiguchi,^{18,†} H. Sekiya,^{49,*} M. Shibata,^{18,†} Y. Shimizu,⁵⁰ M. Shiozawa,^{49,*} S. Short,²¹
P.D. Sinclair,²¹ M. Siyad,⁴⁷ B.M. Smith,²¹ R.J. Smith,³⁶ M. Smy,^{7,*} J.T. Sobczyk,⁵⁹ H. Sobel,^{7,*} M. Sorel,²⁰
A. Stahl,⁴² P. Stamoulis,²⁰ J. Steinmann,⁴² B. Still,³⁹ J. Stone,^{4,*} C. Strabel,¹⁵ R. Sulej,² A. Suzuki,²⁷ K. Suzuki,²⁸
S. Suzuki,^{18,†} S.Y. Suzuki,^{18,†} Y. Suzuki,^{18,†} Y. Suzuki,^{49,*} T. Szegłowski,⁴⁵ M. Szeptycka,² R. Tacik,^{40,52}
M. Tada,^{18,†} M. Taguchi,²⁸ S. Takahashi,²⁸ A. Takeda,^{49,*} Y. Takenaga,⁴⁹ Y. Takeuchi,^{27,*} K. Tanaka,^{18,†}
H.A. Tanaka,^{5,¶} M. Tanaka,^{18,†} M.M. Tanaka,^{18,†} N. Tanimoto,⁵⁰ K. Tashiro,³⁵ I. Taylor,³⁴ A. Terashima,^{18,†}

D. Terhorst,⁴² R. Terri,³⁹ L.F. Thompson,⁴⁴ A. Thorley,³⁰ W. Toki,¹¹ S. Tobayama,⁵ T. Tomaru,^{18,†} Y. Totsuka,^{18,‡}
 C. Touramanis,³⁰ T. Tsukamoto,^{18,†} M. Tzanov,^{31,10} Y. Uchida,²¹ K. Ueno,⁴⁹ A. Vacheret,²¹ M. Vagins,^{7,*}
 G. Vasseur,⁸ O. Veledar,⁴⁴ T. Wachala,¹⁷ J.J. Walding,²¹ A.V. Waldron,³⁶ C.W. Walter,^{13,*} P.J. Wanderer,⁶
 J. Wang,⁴⁸ M.A. Ward,⁴⁴ G.P. Ward,⁴⁴ D. Wark,^{47,21} M.O. Wascko,²¹ A. Weber,^{36,47} R. Wendell,¹³ N. West,³⁶
 L.H. Whitehead,⁵⁶ G. Wikström,¹⁶ R.J. Wilkes,⁵⁷ M.J. Wilking,⁵² Z. Williamson,³⁶ J.R. Wilson,³⁹ R.J. Wilson,¹¹
 T. Wongjirad,¹³ S. Yamada,⁴⁹ Y. Yamada,^{18,†} A. Yamamoto,^{18,†} K. Yamamoto,³⁵ Y. Yamanoi,^{18,†} H. Yamaoka,^{18,†}
 T. Yamauchi,²⁸ C. Yanagisawa,^{34,‡} T. Yano,²⁷ S. Yen,⁵² N. Yershov,²⁶ M. Yokoyama,^{48,*} T. Yuan,¹⁰ A. Zalewska,¹⁷
 J. Zalipska,⁵ L. Zambelli,³⁷ K. Zaremba,⁵⁵ M. Ziembicki,⁵⁵ E.D. Zimmerman,¹⁰ M. Zito,⁸ and J. Żmuda⁵⁹

(The T2K Collaboration)

¹University of Alberta, Centre for Particle Physics, Department of Physics, Edmonton, Alberta, Canada

²National Center for Nuclear Research, Warsaw, Poland

³University of Bern, Albert Einstein Center for Fundamental Physics,
 Laboratory for High Energy Physics (LHEP), Bern, Switzerland

⁴Boston University, Department of Physics, Boston, Massachusetts, U.S.A.

⁵University of British Columbia, Department of Physics and Astronomy, Vancouver, British Columbia, Canada

⁶Brookhaven National Laboratory, Physics Department, Upton, New York, U.S.A.

⁷University of California, Irvine, Department of Physics and Astronomy, Irvine, California, U.S.A.

⁸IRFU, CEA Saclay, Gif-sur-Yvette, France

⁹Chonnam National University, Institute for Universe & Elementary Particles, Gwangju, Korea

¹⁰University of Colorado at Boulder, Department of Physics, Boulder, Colorado, U.S.A.

¹¹Colorado State University, Department of Physics, Fort Collins, Colorado, U.S.A.

¹²Dongshin University, Department of Physics, Naju, Korea

¹³Duke University, Department of Physics, Durham, North Carolina, U.S.A.

¹⁴Ecole Polytechnique, IN2P3-CNRS, Laboratoire Leprince-Ringuet, Palaiseau, France

¹⁵ETH Zurich, Institute for Particle Physics, Zurich, Switzerland

¹⁶University of Geneva, Section de Physique, DPNC, Geneva, Switzerland

¹⁷H. Niewodniczanski Institute of Nuclear Physics PAN, Cracow, Poland

¹⁸High Energy Accelerator Research Organization (KEK), Tsukuba, Ibaraki, Japan

¹⁹Institut de Fisica d'Altes Energies (IFAE), Bellaterra (Barcelona), Spain

²⁰IFIC (CSIC & University of Valencia), Valencia, Spain

²¹Imperial College London, Department of Physics, London, United Kingdom

²²INFN Sezione di Bari and Università e Politecnico di Bari, Dipartimento Interuniversitario di Fisica, Bari, Italy

²³INFN Sezione di Napoli and Università di Napoli, Dipartimento di Fisica, Napoli, Italy

²⁴INFN Sezione di Padova and Università di Padova, Dipartimento di Fisica, Padova, Italy

²⁵INFN Sezione di Roma and Università di Roma "La Sapienza", Roma, Italy

²⁶Institute for Nuclear Research of the Russian Academy of Sciences, Moscow, Russia

²⁷Kobe University, Kobe, Japan

²⁸Kyoto University, Department of Physics, Kyoto, Japan

²⁹Lancaster University, Physics Department, Lancaster, United Kingdom

³⁰University of Liverpool, Department of Physics, Liverpool, United Kingdom

³¹Louisiana State University, Department of Physics and Astronomy, Baton Rouge, Louisiana, U.S.A.

³²Université de Lyon, Université Claude Bernard Lyon 1, IPN Lyon (IN2P3), Villeurbanne, France

³³Miyagi University of Education, Department of Physics, Sendai, Japan

³⁴State University of New York at Stony Brook, Department of Physics and Astronomy, Stony Brook, New York, U.S.A.

³⁵Osaka City University, Department of Physics, Osaka, Japan

³⁶Oxford University, Department of Physics, Oxford, United Kingdom

³⁷UPMC, Université Paris Diderot, CNRS/IN2P3, Laboratoire de

Physique Nucléaire et de Hautes Energies (LPNHE), Paris, France

³⁸University of Pittsburgh, Department of Physics and Astronomy, Pittsburgh, Pennsylvania, U.S.A.

³⁹Queen Mary, University of London, School of Physics and Astronomy, London, United Kingdom

⁴⁰University of Regina, Department of Physics, Regina, Saskatchewan, Canada

⁴¹University of Rochester, Department of Physics and Astronomy, Rochester, New York, U.S.A.

⁴²RWTH Aachen University, III. Physikalisches Institut, Aachen, Germany

⁴³Seoul National University, Department of Physics and Astronomy, Seoul, Korea

⁴⁴University of Sheffield, Department of Physics and Astronomy, Sheffield, United Kingdom

⁴⁵University of Silesia, Institute of Physics, Katowice, Poland

⁴⁶STFC, Daresbury Laboratory, Warrington, United Kingdom

⁴⁷STFC, Rutherford Appleton Laboratory, Harwell Oxford, United Kingdom

⁴⁸University of Tokyo, Department of Physics, Tokyo, Japan

⁴⁹University of Tokyo, Institute for Cosmic Ray Research, Kamioka Observatory, Kamioka, Japan

⁵⁰University of Tokyo, Institute for Cosmic Ray Research, Research Center for Cosmic Neutrinos, Kashiwa, Japan

⁵¹University of Toronto, Department of Physics, Toronto, Ontario, Canada

⁵²TRIUMF, Vancouver, British Columbia, Canada

⁵³University of Victoria, Department of Physics and Astronomy, Victoria, British Columbia, Canada

⁵⁴University of Warsaw, Faculty of Physics, Warsaw, Poland

⁵⁵Warsaw University of Technology, Institute of Radioelectronics, Warsaw, Poland

⁵⁶University of Warwick, Department of Physics, Coventry, United Kingdom

⁵⁷University of Washington, Department of Physics, Seattle, Washington, U.S.A.

⁵⁸University of Winnipeg, Department of Physics, Winnipeg, Manitoba, Canada

⁵⁹Wroclaw University, Faculty of Physics and Astronomy, Wroclaw, Poland

⁶⁰York University, Department of Physics and Astronomy, Toronto, Ontario, Canada

(Dated: November 15, 2018)

We report a measurement of muon-neutrino disappearance in the T2K experiment. The 295-km muon-neutrino beam from Tokai to Kamioka is the first implementation of the off-axis technique in a long-baseline neutrino oscillation experiment. With data corresponding to 1.43×10^{20} protons on target, we observe 31 fully-contained single μ -like ring events in Super-Kamiokande, compared with an expectation of 104 ± 14 (syst) events without neutrino oscillations. The best-fit point for two-flavor $\nu_\mu \rightarrow \nu_\tau$ oscillations is $\sin^2(2\theta_{23}) = 0.98$ and $|\Delta m_{32}^2| = 2.65 \times 10^{-3} \text{ eV}^2$. The boundary of the 90% confidence region includes the points $(\sin^2(2\theta_{23}), |\Delta m_{32}^2|) = (1.0, 3.1 \times 10^{-3} \text{ eV}^2)$, $(0.84, 2.65 \times 10^{-3} \text{ eV}^2)$ and $(1.0, 2.2 \times 10^{-3} \text{ eV}^2)$.

PACS numbers: 14.60.Pq, 13.15.+g, 25.30.Pt, 95.55.Vj

We report a measurement of muon-neutrino disappearance in the T2K experiment. The muon-neutrino beam from Tokai to Kamioka is the first implementation of the off-axis technique [1] in a long-baseline neutrino oscillation experiment. The off-axis technique is used to provide a narrow-band neutrino energy spectrum tuned to the value of L/E that maximizes the neutrino oscillation effect due to Δm_{32}^2 , the mass splitting first observed in atmospheric neutrinos [2]. This narrow-band energy spectrum also provides a clean signature for subdominant electron neutrino appearance, as we have recently reported [3]. Muon-neutrino disappearance depends on the survival probability, which, in the framework of two-flavor $\nu_\mu \rightarrow \nu_\tau$ oscillations, is given by

$$P_{surv} = 1 - \sin^2(2\theta_{23}) \sin^2\left(\frac{\Delta m_{32}^2 L}{4E}\right), \quad (1)$$

where E is the neutrino energy and L is the neutrino propagation length. We have neglected subleading oscillation terms. In this paper we describe our observation of ν_μ disappearance, and we use the result to measure $|\Delta m_{32}^2|$ and $\sin^2(2\theta_{23})$. Previous measurements of these neutrino mixing parameters have been reported by K2K [4] and MINOS [5], which use on-axis neutrino beams, and Super-Kamiokande [6], which uses atmospheric neutrinos.

Details of the T2K experimental setup are described elsewhere [7]. Here we briefly review the components relevant for the ν_μ oscillation analysis. The J-PARC Main Ring (MR) accelerator [8] provides 30 GeV protons with a cycle of 0.3 Hz. Six bunches (Run 1) or eight bunches (Run 2) are extracted in a 5- μ s spill and are transported to the production target through an arc instrumented by superconducting magnets. The proton beam position, profile, timing and intensity are measured by 21 elec-

trostatic beam position monitors (ESM), 19 segmented secondary emission monitors (SSEM), one optical transition radiation monitor (OTR) and five current transformers. The secondary beamline, filled with helium at atmospheric pressure, is composed of the target, focusing horns and decay tunnel. The graphite target is 2.6 cm in diameter and 90 cm ($1.9 \lambda_{int}$) long. Positively-charged particles exiting the target are focused into the 96-m long decay tunnel by three magnetic horns pulsed at 250 kA. Neutrinos are primarily produced in the decays of charged pions and kaons. A beam dump is located at the end of the tunnel and is followed by muon monitors measuring the beam direction of each spill.

The neutrino beam is directed 2.5° off the axis between the target and the Super-Kamiokande (SK) far detector 295 km away. This configuration produces a narrow-band ν_μ beam with peak energy tuned to the first oscillation maximum $E_\nu = |\Delta m_{32}^2|L/(2\pi) \simeq 0.6 \text{ GeV}$.

The near detector complex (ND280) [7] is located 280 m downstream from the target and hosts two detectors. The on-axis Interactive Neutrino GRID (IN-GRID) [9] records neutrino interactions with high statistics to monitor the beam intensity, direction and profile. It consists of 14 identical 7-ton modules composed of an iron-absorber/scintillator-tracker sandwich arranged in 10 m by 10 m crossed horizontal and vertical arrays centered on the beam. The off-axis detector reconstructs exclusive final states to study neutrino interactions and beam properties corresponding to those expected at the far detector. Embedded in the refurbished UA1/NOMAD magnet (field strength 0.2 T), it consists of three large-volume time projection chambers (TPCs) [10] interleaved with two fine-grained tracking detectors (FGDs, each 1 ton). It also has a π^0 -optimized detector and a surrounding electromagnetic calorimeter.

The magnet yoke is instrumented as a side muon range detector.

The SK water-Cherenkov far detector [11] has a fiducial volume (FV) of 22.5 kt within its cylindrical inner detector (ID). Enclosing the ID is the 2 m-wide outer detector (OD). The front-end readout electronics [7] allow for a dead-time-free trigger. Spill timing information, synchronized by the Global Positioning System (GPS) with < 150 ns precision, is transferred from J-PARC to SK and triggers the recording of photomultiplier (PMT) hits within ± 500 μ s of the expected neutrino arrival time.

The results presented in this Letter are based on the first two physics runs: Run 1 (Jan–Jun 2010) and Run 2 (Nov 2010–Mar 2011). During this time period, the MR proton beam power was continually increased and reached 145 kW with 9×10^{13} protons per pulse. The fraction of protons hitting the target was monitored by the ESM, SSEM and OTR and found to be greater than 99% and stable in time. A total of 2,474,419 spills was retained for analysis after beam and far-detector quality cuts, corresponding to 1.43×10^{20} protons on target (POT).

We present the study of events in the far detector with a single muon-like (μ -like) ring. The event selection enhances ν_μ charged-current quasi-elastic interactions (CCQE). For these events, neglecting the Fermi motion, the neutrino energy E_ν can be reconstructed as

$$E_\nu = \frac{m_p^2 - (m_n - E_b)^2 - m_\mu^2 + 2(m_n - E_b)E_\mu}{2(m_n - E_b - E_\mu + p_\mu \cos \theta_\mu)}, \quad (2)$$

where m_p is the proton mass, m_n the neutron mass, and $E_b = 27$ MeV the binding energy of a nucleon inside a ^{16}O nucleus. In Eq. 2 E_μ , p_μ , and θ_μ are respectively the measured muon energy, momentum and angle with respect to the incoming neutrino. The selection criteria for this analysis were fixed from Monte Carlo (MC) studies before the data were collected. The observed number of events and spectrum are compared with signal and background expectations, which are based on neutrino flux and cross-section predictions and are corrected using an inclusive measurement in the off-axis near detector.

Our predicted beam flux (Fig. 1) is based on models tuned to experimental data. The most significant constraint comes from NA61 measurements of pion production [12] in (p, θ) bins, where p is the pion momentum and θ the polar angle with respect to the proton beam; there are 5%-10% systematic and similar statistical uncertainties in most of the measured phase space. The production of pions in the target outside the NA61-measured phase space and all kaon production are modeled using FLUKA [13, 14]. The production rate of these pions is assigned systematic uncertainties of 50%, and kaon production uncertainties are estimated to be between 15% and 100% based on a comparison of FLUKA with data from Eichten et al. [15]. The software package GEANT3 [16], with

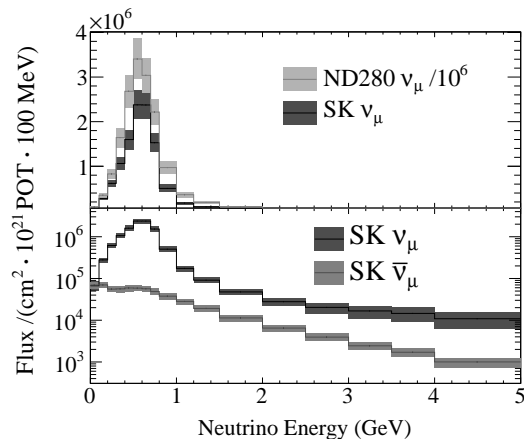


FIG. 1. (Top) The predicted flux of ν_μ as a function of neutrino energy without oscillations at Super-Kamiokande and at the off-axis near detector; (Bottom) the flux of ν_μ and $\bar{\nu}_\mu$ at Super-Kamiokande. The shaded boxes indicate the total systematic uncertainty for each energy bin.

GCALOR [17] for hadronic interactions, handles particle propagation through the magnetic horns, target hall, decay volume and beam dump. Additional systematic errors in the neutrino fluxes are included for uncertainties in secondary nucleon production and total hadronic inelastic cross sections, uncertainties in the proton beam direction, spatial extent and angular divergence, the horn current, and the secondary beam line component alignment uncertainties. The stability of the beam direction and neutrino rate per proton on target are monitored continuously with INGRID and are within the assigned systematic uncertainties [3].

Systematic uncertainties in the shape of the flux as a function of neutrino energy require knowledge of the correlations of the uncertainties in (p, θ) bins of hadron production. For the NA61 pion-production data [12], we assume full correlation between (p, θ) bins for each individual source of systematic uncertainty, except for particle identification where there is a known momentum-dependent correlation. Where correlations of hadron-production uncertainties are unknown, we choose correlations in kinematic variables to maximize the uncertainty in the normalization of the predicted flux.

Neutrino interactions are simulated using the NEUT event generator [18]. Uncertainties in cross sections of the exclusive neutrino processes are determined by comparisons with recent measurements from the SciBooNE [19], MiniBooNE [20, 21], and K2K [22, 23] experiments, comparisons with the GENIE [24] and NuWro [25] generators and recent theoretical work [26].

An inclusive ν_μ charged-current (CC) measurement in the off-axis near detector (ND) is used to constrain the expected event rate at the far detector. From a data sample collected in Run 1 of 2.88×10^{19} POT, neutrino interactions are selected in the FGDs with charged particles entering the downstream TPC. The most energetic neg-

actively charged particle in the TPC is required to have ionization energy loss compatible with that of a muon. The analysis selects 1529 data events with 38% ν_μ CC efficiency and 90% purity. The agreement between the reconstructed neutrino energy in data and MC is shown in Fig. 2. The ratio of measured ν_μ CC interactions to MC is

$$R_{ND}^{\nu_\mu CC} = \frac{N_{ND}^{Data, \nu_\mu CC}}{N_{ND}^{MC, \nu_\mu CC}} = 1.036 \pm 0.028(\text{stat.}) \\ \pm 0.044(\text{det. syst.}) \pm 0.038(\text{phys. syst.}), \quad (3)$$

where $N_{ND}^{Data, \nu_\mu CC}$ is the number of ν_μ CC events, and $N_{ND}^{MC, \nu_\mu CC}$ is the MC prediction normalized by POT. The detector systematic errors in Eq. 3 are mainly due to uncertainties in tracking and particle identification efficiencies. The physics uncertainties result from cross section uncertainties but exclude normalization uncertainties that cancel in a far/near ratio.

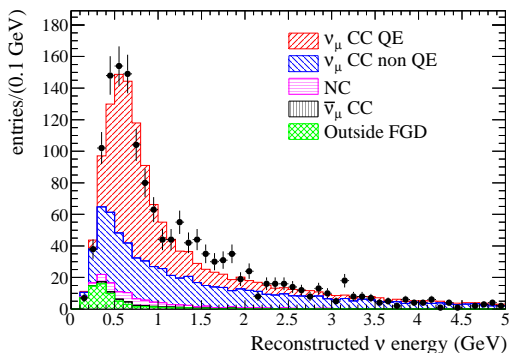


FIG. 2. Neutrino energy reconstructed for the CCQE hypothesis for ν_μ CC candidates interacting in the FGD target. The data are shown using points with error bars (statistical only) and the MC predictions are in shaded histograms.

At the far detector we select a ν_μ CCQE enriched sample. The SK event reconstruction [27] uses PMT hits in time with a neutrino spill. We select a fully-contained fiducial volume (FCFV) sample by requiring no activity in the OD, no pre-activity in the 100 μ s before the event trigger time, at least 30 MeV electron-equivalent energy deposited in the ID, and a reconstructed event vertex in the fiducial region. The OD veto rejects events induced by neutrino interactions outside of the ID, and events where energy escapes from the ID. The visible energy requirement rejects events from radioactive decays in the detector. The fiducial vertex requirement rejects particles entering from outside the ID. Further conditions are required to enrich the sample in ν_μ CCQE events: a single Cherenkov ring identified as a muon, with momentum $p_\mu > 200$ MeV/c, and no more than one delayed electron. The muon momentum requirement rejects charged pions and misidentified electrons from the decay of un-

TABLE I. Event reduction at the far detector. After each selection criterion is applied, the number of observed (Data) and MC expected events of ν_μ CCQE, ν_μ CC non-QE, intrinsic ν_e , and neutral current (NC) are given. The columns denoted by ν_μ include $\bar{\nu}_\mu$. All MC CC samples assume $\nu_\mu \rightarrow \nu_\tau$ oscillations with $\sin^2(2\theta_{23})=1.0$ and $|\Delta m_{32}^2|=2.4 \times 10^{-3} \text{eV}^2$.

	Data	ν_μ CCQE	ν_μ CC non-QE	ν_e CC	NC
FV interaction	n/a	24.0	43.7	3.1	71.0
FCFV	88	19.0	33.8	3.0	18.3
single ring	41	17.9	13.1	1.9	5.7
μ -like	33	17.6	12.4	<0.1	1.9
$p_\mu > 200$ MeV/c	33	17.5	12.4	<0.1	1.9
0 or 1 delayed e	31	17.3	9.2	<0.1	1.8

seen muons and pions, and the delayed-electron veto rejects events with muons accompanied by unseen pions and muons. The number of events in data and MC after each selection criterion is shown in Table I. The efficiency and purity of ν_μ CCQE events are estimated to be 72% and 61% respectively.

We calculate the expected number of signal events in the far detector (N_{SK}^{exp}) by correcting the far-detector MC prediction with $R_{ND}^{\nu_\mu CC}$ from Eq. 3:

$$N_{SK}^{exp}(E_r) = R_{ND}^{\nu_\mu CC} \sum_{E_t} P_{surv}(E_t) N_{SK}^{MC}(E_r, E_t). \quad (4)$$

In Eq. 4, $N_{SK}^{MC}(E_r, E_t)$ is the expected number of events for the no-disappearance hypothesis for T2K Runs 1 and 2 in bins of reconstructed (E_r) and true (E_t) energies. $P_{surv}(E_t)$ is the two-flavor ν_μ -survival probability, and is applied to ν_μ and $\bar{\nu}_\mu$ CC interactions but not to neutral-current interactions.

The sources of systematic uncertainty in N_{SK}^{exp} are listed in Table II. Uncertainties in the near-detector and far-detector selection efficiencies are energy-independent except for the ring-counting efficiency. Uncertainty in the near-detector event rate is applied to $N_{ND}^{Data, \nu_\mu CC}$ in Eq. 3. The flux normalization uncertainty is reduced because of the near-detector constraint. The uncertainty in the flux shape is propagated using the covariance matrix when calculating N_{SK}^{exp} . The near-detector constraint also leads to partial cancellation in the uncertainty in cross section modeling, but the cancellation is not complete due to the different fluxes, different acceptances and different nuclei in the near and far detectors. The total uncertainty in N_{SK}^{exp} is $+13.3\%$ without oscillations and $+15.0\%$ with oscillations with $\sin^2(2\theta_{23}) = 1.0$ and $|\Delta m_{32}^2| = 2.4 \times 10^{-3} \text{eV}^2$.

We find the best-fit values of the oscillation parameters using a binned likelihood-ratio method, in which $\sin^2(2\theta_{23})$ and $|\Delta m_{32}^2|$ are varied in the input to the cal-

TABLE II. Systematic uncertainties on the predicted number of SK selected events without oscillations and for oscillations with $\sin^2(2\theta_{23}) = 1.0$ and $|\Delta m_{32}^2| = 2.4 \times 10^{-3} \text{ eV}^2$.

Source	$\delta N_{SK}^{exp}/N_{SK}^{exp}$ (%, no osc)	$\delta N_{SK}^{exp}/N_{SK}^{exp}$ (%, with osc)
SK CCQE efficiency	± 3.4	± 3.4
SK CC non-QE efficiency	± 3.3	± 6.5
SK NC efficiency	± 2.0	± 7.2
ND280 efficiency	+5.5 -5.3	+5.5 -5.3
ND280 event rate	± 2.6	± 2.6
Flux normalization (SK/ND280)	± 7.3	± 4.8
CCQE cross section	± 4.1	± 2.5
CC1 π /CCQE cross section	+2.2 -1.9	+0.4 -0.5
Other CC/CCQE cross section	+5.3 -4.7	+4.1 -3.6
NC/CCQE cross section	± 0.8	± 0.9
Final-state interactions	± 3.2	± 5.9
Total	+13.3 -13.0	+15.0 -14.8

culuation of N_{SK}^{exp} until

$$2 \sum_{E_r} \left[N_{SK}^{data} \ln \left(\frac{N_{SK}^{data}}{N_{SK}^{exp}} \right) + (N_{SK}^{exp} - N_{SK}^{data}) \right] \quad (5)$$

is minimized. The sum in Eq. 5 is over 50 MeV bins of reconstructed energy of selected events in the far detector from 0-10 GeV.

Using the near-detector measurement and setting $P_{surv} = 1.0$ in Eq. 4, we expect a total of $103.6^{+13.8}_{-13.4}$ (syst) single μ -like ring events in the far detector without disappearance, but we observe 31 events. If $\nu_\mu \rightarrow \nu_\tau$ oscillations are assumed, the best-fit point determined using Eq. 5 is $\sin^2(2\theta_{23}) = 0.98$ and $|\Delta m_{32}^2| = 2.65 \times 10^{-3} \text{ eV}^2$. We estimate the systematic uncertainty in the best-fit value of $\sin^2(2\theta_{23})$ to be $\pm 4.7\%$ and that in $|\Delta m_{32}^2|$ to be $\pm 4.5\%$. The reconstructed energy spectrum of the 31 data events is shown in Fig. 3 along with the expected far-detector spectra without disappearance and with best-fit oscillations.

We construct confidence regions¹ in the oscillation parameters using the method of Feldman and Cousins [28]. Statistical variations are taken into account by Poisson fluctuations of toy MC datasets, and systematic uncertainties are incorporated using the method of Cousins and Highland [29, 30]. The 90% confidence region for $\sin^2(2\theta_{23})$ and $|\Delta m_{32}^2|$ is shown in Fig. 4 for combined statistical and systematic uncertainties.

¹ In the T2K narrow-band beam, for a low-statistics data set, there is a possible degeneracy between the first oscillation maximum and other oscillation maxima in L/E . Therefore we decided in advance to report confidence regions both with and without an explicit bound at $|\Delta m_{32}^2| < 5 \times 10^{-3} \text{ eV}^2$. For this data set, the bounded and unbounded confidence regions are identical.

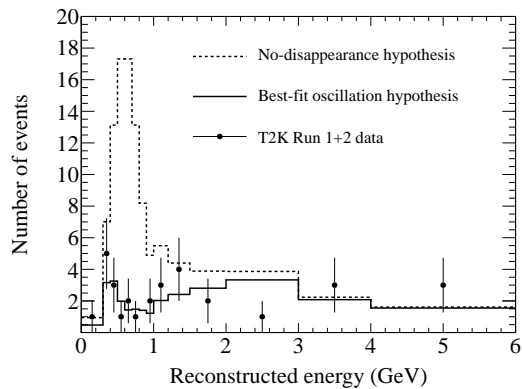


FIG. 3. Reconstructed energy spectrum of the 31 data events compared with the expected spectra in the far detector without disappearance and with best-fit $\nu_\mu \rightarrow \nu_\tau$ oscillations. A variable binning scheme is used here for the purpose of illustration only; the actual analysis used equal-sized 50 MeV bins.

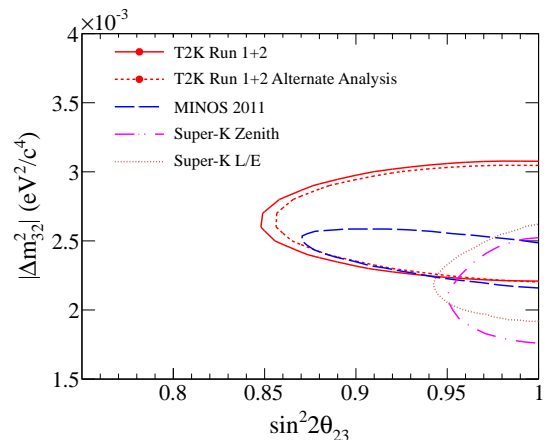


FIG. 4. The 90% confidence regions for $\sin^2(2\theta_{23})$ and $|\Delta m_{32}^2|$; results from the two analyses reported here are compared with those from MINOS [5] and Super-Kamiokande [6, 31].

We also carried out an alternate analysis with a maximum likelihood method. The likelihood is defined as:

$$L = L_{\text{norm}}(\sin^2(2\theta_{23}), \Delta m_{32}^2, \mathbf{f}) L_{\text{shape}}(\sin^2(2\theta_{23}), \Delta m_{32}^2, \mathbf{f}) L_{\text{sys}}(\mathbf{f}), \quad (6)$$

where the first term is the Poisson probability for the observed number of events, and the second term is the unbinned likelihood for the reconstructed neutrino energy spectrum. The vector \mathbf{f} represents parameters related to systematic uncertainties that have been allowed to vary in the fit to maximize the likelihood, and the last term in Eq. 6 is a multidimensional Gaussian probability for the systematic error parameters. The result is consistent with the analysis described earlier. The best-fit point for this alternate analysis is $\sin^2(2\theta_{23}) = 0.99$ and $|\Delta m_{32}^2| = 2.63 \times 10^{-3} \text{ eV}^2$. The 90% confidence region for the neutrino oscillation parameters is shown in Fig. 4.

In conclusion, we have reported the first observation

of ν_μ disappearance using detectors positioned off-axis in the beam of a long-baseline neutrino experiment. The values of the oscillation parameters $\sin^2(2\theta_{23})$ and $|\Delta m_{32}^2|$ obtained are consistent with those reported by MINOS [5] and Super-Kamiokande [6, 31].

We thank the J-PARC accelerator team for the superb accelerator performance and CERN NA61 colleagues for providing essential particle production data and for their fruitful collaboration. We acknowledge the support of MEXT, Japan; NSERC, NRC and CFI, Canada; CEA and CNRS/IN2P3, France; DFG, Germany; INFN, Italy; Ministry of Science and Higher Education, Poland; RAS, RFBR and the Ministry of Education and Science of the Russian Federation; MEST and NRF, South Korea; MICINN and CPAN, Spain; SNSF and SER, Switzerland; STFC, U.K.; NSF and DOE, U.S.A. We also thank CERN for their donation of the UA1/NOMAD magnet and DESY for the HERA-B magnet mover system. In addition, participation of individual researchers and institutions in T2K has been further supported by funds from: ERC (FP7), EU; JSPS, Japan; Royal Society, UK; DOE Early Career program, and the A. P. Sloan Foundation, U.S.A.

* also at IPMU, TODIAS, Univ. of Tokyo, Japan

† also at J-PARC Center

‡ deceased

§ now at CERN

¶ also at Institute of Particle Physics, Canada

** also at IPMU, TODIAS, Univ. of Tokyo, Japan; also at J-PARC Center

†† also at JINR, Dubna, Russia

‡‡ also at BMCC/CUNY, New York, New York, U.S.A.

- [1] D. Beavis et al. (E889 Collaboration), Physics Design Report **BNL 52459** (1995).
 [2] Y. Fukuda et al. (Super-Kamiokande Collaboration), Phys. Rev. Lett. **81**, 1562 (1998).
 [3] K. Abe et al. (T2K Collaboration), Phys. Rev. Lett. **107**, 041801 (2011).
 [4] M.H. Ahn et al. (K2K Collaboration), Phys. Rev. D **74**, 072003 (2006).
 [5] P. Adamson et al. (MINOS Collaboration), Phys. Rev.

Lett. **106**, 181801 (2011).

- [6] K. Abe et al. (Super-Kamiokande Collaboration), submitted to Phys. Rev. Lett. (2011), hep-ex/1109.1621.
 [7] K. Abe et al. (T2K Collaboration), Nucl. Instrum. Meth. **A659**, 106 (2011).
 [8] Y. Yamazaki et al., KEK Report 2002-13 and JAERI-Tech 2003-44 and J-PARC-03-01 (2003).
 [9] K. Abe et al. (T2K Collaboration), submitted to Nucl. Instrum. Meth. (2011), arXiv:1111.3119.
 [10] N. Abgrall et al., Nucl. Instrum. Meth. **A637**, 25 (2011).
 [11] Y. Fukuda et al. (Super-Kamiokande Collaboration), Nucl. Instrum. Meth. **A501**, 418 (2003).
 [12] N. Abgrall et al. (NA61/SHINE Collaboration), Phys.Rev.C **84**, 034604 (2011).
 [13] A. Ferrari, P. R. Sala, A. Fasso, and J. Ranft, (2005), CERN-2005-010 and SLAC-R-773 and INFN-TC-05-11.
 [14] G. Battistoni et al., AIP Conf. Proc. **896**, 31 (2007).
 [15] T. Eichten et al., Nucl. Phys. B **44**, 333 (1972).
 [16] R. Brun, F. Carminati, and S. Giani, (1994), CERN-W5013.
 [17] C. Zeitnitz and T. A. Gabriel, In Proc. of International Conference on Calorimetry in High Energy Physics, Tallahassee, FL, USA, February 1993.
 [18] Y. Hayato, Acta Phys.Polon. **B40**, 2477 (2009).
 [19] J. Alcaraz-Aunon and J. Walding (SciBooNE Collaboration), AIP Conf. Proc. **1189**, 145 (2009).
 [20] A. A. Aguilar-Arevalo et al. (MiniBooNE Collaboration), Phys.Rev. **D81**, 092005 (2010).
 [21] A. A. Aguilar-Arevalo et al. (MiniBooNE Collaboration), Phys.Rev.Lett. **103**, 081801 (2009).
 [22] R. Gran et al. (K2K Collaboration), Phys. Rev. D **74**, 052002 (2006).
 [23] A. Rodriguez et al. (K2K Collaboration), Phys. Rev. D **78**, 032003 (2008).
 [24] C. Andreopoulos et al., Nucl.Instrum.Meth. **A614**, 87 (2010).
 [25] C. Juszczak, Acta Phys. Polon. **840**, 2507 (2009).
 [26] C. Juszczak et al., Phys. Rev. C **82**, 045502 (2010).
 [27] Y. Ashie et al. (Super-Kamiokande Collaboration), Phys. Rev. **D71**, 112005 (2005).
 [28] G. J. Feldman and R. D. Cousins, Phys. Rev. D **57**, 3873 (1998).
 [29] R. Cousins and V. Highland, Nucl. Instrum. Meth. **A320**, 331 (1992).
 [30] J. Conrad, O. Botner, A. Hallgren, and C. Perez de los Heros, Phys.Rev. **D67**, 012002 (2003).
 [31] Y. Takeuchi (Super-Kamiokande Collaboration), to be published in Proceedings of Neutrino 2010..